AIAA JOURNAL
Vol. 37, No. 2, February 1999

# Thermoviscoelastic Analysis of Composite Structures Using a Triangular Flat Shell Element

Daniel C. Hammerand* and Rakesh K. Kapania†
*Virginia Polytechnic Institute and State University, Blacksburg, Virginia 24061-0203*

**To accurately model the structural response of fiber-reinforced polymer-matrix composites, it is necessary to account for viscoelastic behavior of the polymer matrix. Therefore, the geometrically linear dynamic analysis capability of a recently developed triangular flat shell element for elastic composite structures is extended here to include thermoviscoelasticity. The flat shell element is the combination of the discrete Kirchhoff theory plate bending element and a membrane element similar to the Allman triangle, but derived by transforming the linear strain triangle element. Linear viscoelastic composite materials are modeled, resulting in the relaxation moduli being expressed as Prony series. Hygrothermorheologically simple materials are considered for which a change in the hygrothermal environment results in a horizontal shifting of the relaxation moduli curves on a log timescale, in addition to the usual hygrothermal loads. The resulting hereditary integral terms are evaluated using a recursion relationship requiring only the previous two solutions. The Newmark method is used to incorporate the inertia terms. Numerical examples are presented to demonstrate the accuracy of the present formulation when compared with correspondence principle solutions and results available in the literature.**

## Introduction

EXAMPLES of viscoelastic materials include metals at high temperatures, concrete, and polymers. For fiber-reinforced polymer-matrix composites, the polymer matrix is typically viscoelastic, whereas the fibers are elastic. For polymers, the elastic part of the material response results from the polymer chains being stretched by the applied stress. The viscous response of polymers results from several relaxation mechanisms, such as motion of side-chain groups, reorientation of chain segments relative to each other, and the translation of entire molecules past one another in the case of linear amorphous polymers in the rubbery-flow region.[1] Increasing the temperature and moisture results in the viscous response being accelerated, as has been observed experimentally.[2]

For most amorphous polymers, experiments indicate that changing the temperature and moisture results in a simple horizontal shifting of the relaxation modulus on a log timescale. Such materials are referred to as being hygrothermorheologically simple. For these materials, the relaxation modulus (viscoelastic stress response to a unit applied strain) at the real temperature $T$, moisture $H$, and time $t$ can be related to the relaxation modulus at the reference temperature $T_{\text{ref}}$, reference moisture $H_{\text{ref}}$, and reduced time $\zeta$ by

$$E(T, H, t) = E(T_{\text{ref}}, H_{\text{ref}}, \zeta) \tag{1}$$

where the reduced time and the real time are related by the horizontal shift factor $A_{TH}$ as follows:

$$\zeta = \int_0^t \frac{\mathrm{d}t'}{A_{TH}[T(t'), H(t')]} \tag{2}$$

Although often found to be accurate, a simple horizontal shifting is not valid for multiphase or semicrystalline polymers in general. For two-phase polymers, horizontal shifting alone still will be accurate if there is one dominant phase. In addition to using horizontal shifting, vertical shifting can be included in accounting for the effects of physical aging or semicrystallization. Besides hastening its viscous response, increasing a polymer's temperature leads to an increase in the elastic stiffness of a rubbery network and a decrease in the density $\rho$ that will decrease the relaxation modulus, because the relaxation modulus obviously depends on the amount of matter per unit cross-sectional area.[1] This results in an additional vertical shifting, with the vertical shift factor $\rho T/\rho_{\text{ref}} T_{\text{ref}}$ multiplying the right-hand side of Eq. (1).[1]

Received March 16, 1998; presented as Paper 98-1763 at the AIAA/ASME/ASCE/AHS/ASC 39th Structures, Structural Dynamics, and Materials Conference, Long Beach, CA, April 20–23, 1998; revision received Oct. 1, 1998; accepted for publication Oct. 6, 1998. 

*Graduate Research Assistant, Department of Aerospace and Ocean Engineering. Student Member AIAA.
†Professor, Department of Aerospace and Ocean Engineering. Associate Fellow AIAA.

## Related Works

Linear viscoelastic stress analysis can be performed in the time, complex frequency, or Laplace domains. For general load histories (including hygrothermal loads) and viscoelastic material properties, direct time integration schemes appear to be the most robust. Furthermore, the incorporation of inertia terms presents no additional difficulty. When direct integration schemes were first formulated, they required relatively large amounts of storage to retain all of the previous solutions needed to evaluate the current values of the viscoelastic memory loads.[3] This deficiency in the method was remedied by the development of recursion relationships for these loads.[4–6] One remaining disadvantage of evaluating viscoelastic finite element equations directly in the time domain is that a large number of time steps is needed to generate long-term solutions. The time-step size for accurate calculations may need to be relatively small because of possible error propagation. Given the wide availability of computational resources, these time-step size constraints do not appear to be overly restrictive.

In most direct integration schemes, the hereditary integral form of the constitutive law is used to allow easy incorporation of the effects of temperature and moisture upon the material properties. The hereditary integral contains the convolution of a stiffness operator and either the strain or the displacement itself, with a first-order time derivative taken on either the stiffness operator or the strain or displacement. For hygrothermorheologically simple materials, the stiffness operator in the hereditary integral is specified in terms of a reduced timescale. Typically, to evaluate the change in the hereditary integral over a single time step, one of the two terms of the product comprising the integrand is assumed to be constant over a time step and thus is moved outside the integral.

Zak[4] assumed the displacement at a given point to vary linearly over a time step, resulting in a constant velocity in the integrand. The stiffness operator then was assumed to be constant over a time step, with its value taken to be that at the initial endpoint of the time step. In the hereditary integral formulation used by White,[5] the time derivative was taken to act on the stiffness operator. Assuming the rate of change of the stiffness operator to be constant over a time step, the hereditary integral over a time step reduced to an integration of the strain over the time step, which was performed

using the trapezoidal rule. Another direct integration scheme was proposed by Taylor et al.[6] Similar to that of Zak,[4] Taylor et al.[6] assumed a constant velocity at a given point over a time step. The remaining integral of the stiffness operator over the time step was evaluated exactly for the case where the horizontal shift factor was constant over the time step.

In each case, expressing the stiffness operators in terms of an exponential series allows recursion relationships involving quantities from only the previous two time steps to be used to evaluate the current value of the viscoelastic memory terms, resulting in minimum storage. Of the three direct integration schemes discussed, the method proposed by Taylor et al.[6] appears to be the most accurate because it exactly evaluates the integral of the stiffness operator over a time step for a constant horizontal shift factor over the time step, whereas that integration is never exact in the methods proposed by Zak[4] and White.[5] Thus, the direct integration method of Taylor et al.[6] is chosen for the present development.

Zak[4] analyzed the thermoviscoelastic response of solid-rocket grains under transient thermal loads using a finite difference scheme for the spatial discretization. Taylor et al.[6] developed finite element equations from the application of a variational principle for isotropic thermorheologically simple viscoelastic structures with homogeneous time-dependent temperature fields. The temperature field and, hence, the thermal load vector were assumed to be independent of the displacement field. White[5] assumed a homogeneous, isotropic, thermorheologically simple material with a bulk modulus constant in time. In performing the stress analysis of solid propellant grain under transient thermal loads, a linear temperature variation was assumed over each element, with the reduced time for an element determined using its average nodal temperature.[5]

Wang and Tsai[7] used the hereditary integral approximation presented by White[5] to perform isothermal quasistatic and dynamic finite element analyses of homogeneous, isotropic, viscoelastic Mindlin plates. The Newmark method was utilized in incorporating the inertia term.

The integration method proposed by Taylor et al.[6] for linearly viscoelastic, thermorheologically simple materials was extended to a general three-dimensional finite element model by Ben–Zvi.[8] The incremental linear viscoelastic finite element equations presented by Ben–Zvi[8] only require the user to supply a constitutive routine to a finite element code already incorporating an incremental displacement approach. Thus, the full capabilities of such a host code are maintained. Simplifications to two dimensions and extensions to include material and/or geometric nonlinearities can be made.

Using an incremental finite element method, Krishna et al.[9] studied the quasistatic response of electronic packaging structures that have polymer films bonded to elastic substrates. The polymer film was assumed to be linearly viscoelastic and hygrothermorheologically simple. Thermal cycling and moisture diffusion were applied to packaging structures, with Fick's law used to determine the moisture distribution independent of the structural response problem. The incremental formulation, including hygrothermal loads, was developed using the approximation scheme proposed by Taylor et al.[6] to evaluate the hereditary integral in the constitutive law of the viscoelastic film.

Assuming the material for each layer to be thermorheologically simple, Lin and Hwang[10,11] used the integration method of Taylor et al.[6] to evaluate the thermoviscoelastic response of laminated composites. A thermal load vector assuming the laminate temperature to be uniform at any instant of time was included. The contribution of the thermal load vector to the memory load was evaluated in a manner similar to that used for the stiffness terms. The laminates were assumed to be symmetric and under a state of plane stress, with the mechanical loads restricted to be in-plane only. Graphite/epoxy (Gr/Ep) laminates subjected to creep, relaxation, and temperature load histories were studied. Hilton and Yi[12] and Yi and Hilton[13] used a formulation similar to that of Lin and Hwang[10,11] to analyze the dynamic response of hygrothermorheologically simple viscoelastic composite beams and plates. The Newmark average acceleration method was used to incorporate the inertia term. The formulation for the composite beams[12] included both mechanical and hygrothermal loads, whereas the composite plate formulation[13] only accounted for in-plane and transverse mechanical loads. Hygrothermal loads were added for the quasistatic analysis of hygrothermorheologically simple viscoelastic composite plates and shells by Yi et al.[14]

Extending the formulation of Lin and Hwang,[10,11] Lin and Yi[15] evaluated the interlaminar stresses in linear viscoelastic composite laminates in a state of plane strain under mechanical and hygrothermal loads. The laminates were assumed to be hygrothermorheologically simple. In a later study, Yi and Hilton[16] added Fick's law for diffusion to determine the in-plane and interlaminar stresses of hygrothermorheologically simple linear viscoelastic laminates subjected to moisture absorption and desorption.

In the present study, a direct integration scheme similar to that of Taylor et al.[6] is employed to evaluate the hereditary integrals describing the linear viscoelastic behavior of hygrothermorheologically simple laminated plates and shells. The formulation presented is valid for both quasistatic and dynamic analyses of composite plates and shells under mechanical and hygrothermal loads. Five numerical examples are presented, demonstrating the capability and accuracy of the present formulation.

## Formulation

The geometrically linear dynamic analysis capability of the triangular flat shell element developed by Kapania and Mohan[17] is extended here to include hygrothermoviscoelasticity. Flat shell elements are formulated as a simple combination of a plate bending element and a plate membrane element. The shell behavior (geometric coupling of bending and stretching between elements) is achieved through the transformation of element stiffness matrices and load vectors to a single global coordinate system. The present flat shell element combines the discrete Kirchhoff theory (DKT) plate bending element[18] with a membrane element having the same nodal degrees of freedom (DOF) as the Allman triangle (AT) element.[19]

In the DKT element, thin-walled bending behavior is modeled by applying the Kirchhoff hypothesis along the edges of the triangular element. Following Ertas et al.,[20] the transformation suggested by Cook[21] is used to transform the well-known linear strain triangle (LST) element into a membrane element having two displacements and one rotation at each node. That is, the two translations at the midside nodes of the LST element are mapped into in-plane translations and rotations at the corner nodes. The DOF associated with the transformed LST membrane element and DKT bending element are indicated in Fig. 1. Altogether, the triangular flat shell element has three translations and three rotations at each corner node for a total of 18 DOF.

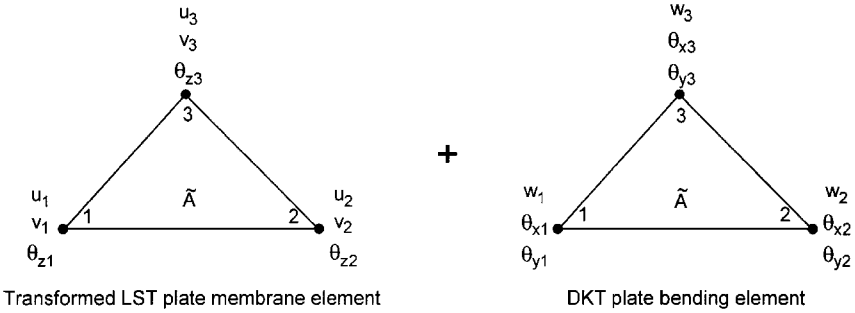


**Fig. 1 Plate membrane and bending elements comprising the triangular flat shell element.**

For an elastic composite under plane stress, including the effects of thermal strains $\{\epsilon^T\}$ and hygroscopic strains $\{\epsilon^H\}$, the stress and strain in a layer relative to a local $x$-$y$ coordinate system are related through the transformed reduced stiffness matrix $[\bar{Q}]$ as

$$\{\sigma\} = [\bar{Q}]\{\epsilon - \epsilon^T - \epsilon^H\} \tag{3}$$

For a hygrothermorheologically simple, linear viscoelastic composite, the corresponding relationship is

$$\{\sigma(t)\} = \int_{-\infty}^{t} [\bar{Q}(\zeta(t) - \zeta'(\tau))]\left\{\frac{\partial \epsilon(\tau)}{\partial \tau} - \frac{\partial \epsilon^T(\tau)}{\partial \tau} - \frac{\partial \epsilon^H(\tau)}{\partial \tau}\right\} \mathrm{d}\tau \tag{4}$$

where reduced timescales must be used in the stiffness operator to account for the temperature and moisture dependence of the material properties. The reduced time $\zeta'$ corresponds to $\tau$ and is defined in a similar fashion as $\zeta$, but with $t$ replaced by $\tau$ in Eq. (2). In the present formulation, no vertical shifting is applied to the relaxation moduli vs time curves.

The element strains $\{\epsilon(t)\}$ are expressed as

$$\{\epsilon(t)\} = \{e(t)\} + z\{\kappa(t)\} = [B_{\mathrm{at}}]\{u(t)\} + z[B_{\mathrm{dkt}}]\{u(t)\} \tag{5}$$

where $z$ is the perpendicular distance from the shell midplane, $[B_{\mathrm{at}}]$ and $[B_{\mathrm{dkt}}]$ are the strain-displacement matrices for the membrane and bending elements, respectively, and $\{u\}$ is the nodal displacement vector for the complete shell element. The thermal and hygroscopic strains for a layer are written, respectively, as

$$\{\epsilon^T(t)\} = \theta_T(t)\{\alpha\}, \qquad \{\epsilon^H(t)\} = \theta_H(t)\{\beta\} \tag{6}$$

where $\{\alpha\}$ and $\{\beta\}$ are the transformed coefficients of thermal and hygroscopic expansion, respectively, and $\theta_T$ and $\theta_H$ are the deviation of the temperature and moisture from thermal-strain-free and hygroscopic-strain-free states, respectively. The present formulation is restricted to the case where the structure's temperature and moisture content are uniform at any instant of time. Equations (5) and (6) hold for both the elastic and viscoelastic cases.

For the elastic case including inertia, the finite element equations before time discretization are written as

$$[M]\{\ddot{U}\} + [K]\{U\} = \{F\} + \{F^T\} + \{F^H\} \tag{7}$$

where $[M]$, $[K]$, $\{F\}$, $\{F^T\}$, $\{F^H\}$, and $\{U\}$ are the assembled global mass matrix, stiffness matrix, mechanical load vector, thermal load vector, hygroscopic load vector, and nodal displacement vector, respectively. The corresponding quantities on the element level are denoted with lowercase letters.

For the hygrothermorheologically simple, linear viscoelastic case, the assembled global finite element equations before time discretization become

$$[M]\{\ddot{U}\} + \int_{-\infty}^{t} [K(\zeta - \zeta')]\left\{\frac{\partial U}{\partial \tau}\right\} \mathrm{d}\tau = \{F\} + \int_{-\infty}^{t} \{F^T(\zeta - \zeta')\}\frac{\partial \theta_T}{\partial \tau}\,\mathrm{d}\tau + \int_{-\infty}^{t} \{F^H(\zeta - \zeta')\}\frac{\partial \theta_H}{\partial \tau}\,\mathrm{d}\tau \tag{8}$$

where the element stiffness kernel and hygrothermal load kernels are

$$[k(\zeta - \zeta')] = \int_{\tilde{A}} \big([B_{\mathrm{at}}]^T[A(\zeta - \zeta')][B_{\mathrm{at}}] + [B_{\mathrm{at}}]^T[B(\zeta - \zeta')][B_{\mathrm{dkt}}] + [B_{\mathrm{dkt}}]^T[B(\zeta - \zeta')][B_{\mathrm{at}}] + [B_{\mathrm{dkt}}]^T[D(\zeta - \zeta')][B_{\mathrm{dkt}}]\big)\,\mathrm{d}\tilde{A} \tag{9}$$

$$\{f^T(\zeta - \zeta')\} = \int_{\tilde{A}} [B_{\mathrm{at}}]^T\left(\int_{z_{\min}}^{z_{\max}} [\bar{Q}(\zeta - \zeta')]\{\alpha\}\,\mathrm{d}z\right)\mathrm{d}\tilde{A} + \int_{\tilde{A}} [B_{\mathrm{dkt}}]^T\left(\int_{z_{\min}}^{z_{\max}} z[\bar{Q}(\zeta - \zeta')]\{\alpha\}\,\mathrm{d}z\right)\mathrm{d}\tilde{A} \tag{10}$$

$$\{f^H(\zeta - \zeta')\} = \int_{\tilde{A}} [B_{\mathrm{at}}]^T\left(\int_{z_{\min}}^{z_{\max}} [\bar{Q}(\zeta - \zeta')]\{\beta\}\,\mathrm{d}z\right)\mathrm{d}\tilde{A} + \int_{\tilde{A}} [B_{\mathrm{dkt}}]^T\left(\int_{z_{\min}}^{z_{\max}} z[\bar{Q}(\zeta - \zeta')]\{\beta\}\,\mathrm{d}z\right)\mathrm{d}\tilde{A} \tag{11}$$

where $\tilde{A}$ is the area of the element and

$$[A(\zeta - \zeta'); B(\zeta - \zeta'); D(\zeta - \zeta')] = \int_{z_{\min}}^{z_{\max}} (1; z; z^2)[\bar{Q}(\zeta - \zeta')]\,\mathrm{d}z \tag{12}$$

The numerical technique for the solution of these equations is similar to the approaches used by Taylor et al.,[6] Lin and Hwang,[10,11] Hilton and Yi,[12,13] and Yi et al.[14] The elastic transformed reduced stiffness matrix is written as

$$[\bar{Q}] = [T]^{-1}\begin{bmatrix} Q_{11} & Q_{12} & 0 \\ Q_{12} & Q_{22} & 0 \\ 0 & 0 & Q_{66} \end{bmatrix}([T]^{-1})^T \tag{13}$$

$$= Q_1[D_1] + Q_2[D_2] + Q_3[D_3] + Q_4[D_4] \tag{14}$$

where the following contracted notation for the reduced stiffnesses is used:

$$Q_1 = Q_{11}, \qquad Q_2 = Q_{12}, \qquad Q_3 = Q_{22}, \qquad Q_4 = Q_{66} \tag{15}$$

and $[D_1]$–$[D_4]$ are determined using

$$[T] = \begin{bmatrix} c^2 & s^2 & 2sc \\ s^2 & c^2 & -2sc \\ -sc & sc & c^2 - s^2 \end{bmatrix} \tag{16}$$

where $c = \cos\theta$, $s = \sin\theta$, and $\theta$ is the angle between the fiber direction and the local $x$ axis.

For linear viscoelasticity, each of the reduced stiffnesses ($Q_1$, $Q_2$, $Q_3$, and $Q_4$) is expressed in terms of Prony series as follows:

$$Q_r(t) = Q_r^{\infty} + \sum_{\rho=1}^{N_r} Q_{r\rho}\, e^{-t/\lambda_{r\rho}} \qquad \text{for} \qquad r = 1, 2, 3, 4 \tag{17}$$

where the $\lambda_{r\rho}$ denote relaxation times governing the material response characteristics. Furthermore, each reduced stiffness is allowed to have its own reduced timescale denoted by $\zeta_r$ and associated horizontal shift factor $A_r$, in order to model the possibility that each reduced stiffness may be affected differently by the hygrothermal environment. Direct substitution of Eq. (17) into Eq. (13) would lead to

$$\left(4 + \sum_{r=1}^{4} N_r\right)$$

transformed reduced stiffness matrices needed for the description of a lamina's behavior. This ultimately would result in

$$\left(4 + \sum_{r=1}^{4} N_r\right)$$

global stiffness matrices and thermal and hygroscopic load vectors that would need to be stored.[10–14] However, substitution of Eq. (17) into Eq. (14) results in the kernel $[\bar{Q}(\zeta - \zeta')]$ of Eq. (4) being expressed in terms of only four matrices ($[D_1]$–$[D_4]$) as follows:

$$[\bar{Q}(\zeta - \zeta')] = \sum_{r=1}^{4}\left(Q_r^{\infty} + \sum_{\rho=1}^{N_r} Q_{r\rho}\exp\left(-\frac{\zeta_r - \zeta_r'}{\lambda_{r\rho}}\right)\right)[D_r] \tag{18}$$

The global stiffness matrix kernel then can be written in a similar fashion as

$$[K(\zeta - \zeta')] = \sum_{r=1}^{4}\left(Q_r^{\infty} + \sum_{\rho=1}^{N_r} Q_{r\rho}\exp\left(-\frac{\zeta_r - \zeta_r'}{\lambda_{r\rho}}\right)\right)[K_r] \tag{19}$$

where $[K_i]$ is the elastic global stiffness matrix for the case in which $Q_i = 1$ and the other three $Q_r$ are zero. Likewise, the kernels for the global thermal and hygroscopic loads are written as

$$\{F^T(\zeta - \zeta')\} = \sum_{r=1}^{4}\left(Q_r^{\infty} + \sum_{\rho=1}^{N_r} Q_{r\rho}\exp\left(-\frac{\zeta_r - \zeta_r'}{\lambda_{r\rho}}\right)\right)\{F_r^T\} \tag{20}$$

$$\{F^H(\zeta - \zeta')\} = \sum_{r=1}^{4}\left(Q_r^{\infty} + \sum_{\rho=1}^{N_r} Q_{r\rho}\exp\left(-\frac{\zeta_r - \zeta_r'}{\lambda_{r\rho}}\right)\right)\{F_r^H\} \tag{21}$$

where $\{F_i^T\}$ and $\{F_i^H\}$ are the elastic global thermal and hygroscopic load vectors, respectively, for the case where $Q_i = 1$ and the other three $Q_r$ are zero.

The integration of a sample hereditary integral over a time step is carried out as follows. Approximating $\{\partial U/\partial\tau\}$ to be constant over a time step and equal to $\{\Delta U^p\}/\Delta t^p$, where $\Delta(\cdot) = (\cdot)^p - (\cdot)^{p-1}$, the following approximation is made:

$$\int_{t^{p-1}}^{t^p}\exp\left(-\frac{\zeta_r^p - \zeta_r'}{\lambda_{r\rho}}\right)Q_{r\rho}[K_r]\left\{\frac{\partial U}{\partial\tau}\right\}\mathrm{d}\tau \approx \bar{S}_{r\rho}^p Q_{r\rho}[K_r]\{\Delta U^p\} \tag{22}$$

where

$$\bar{S}_{r\rho}^p = \frac{1}{\Delta t^p}\int_{t^{p-1}}^{t^p}\exp\left(-\frac{\zeta_r^p - \zeta_r'}{\lambda_{r\rho}}\right)\mathrm{d}\tau \tag{23}$$

Taylor et al.[6] demonstrated the importance of accurately evaluating $\bar{S}_{r\rho}^p$ in controlling numerical error. For the case where $A_r$ is constant over a time step, $\bar{S}_{r\rho}^p$ can be evaluated exactly as[6]

$$\bar{S}_{r\rho}^p = \left(1/\Delta\zeta_r^p\right)\lambda_{r\rho}\left[1 - \exp\left(-\Delta\zeta_r^p/\lambda_{r\rho}\right)\right] \tag{24}$$

Presumably, a sufficiently small time-step size will be used so that Eq. (24) represents an acceptable approximation to Eq. (23) for a given variation in the hygrothermal environment.

The Newmark method is used to represent the current acceleration in terms of the current displacement and the previous displacement, velocity, and acceleration. The current acceleration $\{\ddot{U}^p\}$ is calculated by rearranging the following:

$$\{U^p\} = \{U^{p-1}\} + \Delta t^p\{\dot{U}^{p-1}\} + \tfrac{1}{2}(\Delta t^p)^2\left[(1-\gamma)\{\ddot{U}^{p-1}\} + \gamma\{\ddot{U}^p\}\right] \tag{25}$$

and the current velocity is given by

$$\{\dot{U}^p\} = \{\dot{U}^{p-1}\} + (1-\psi)\Delta t^p\{\ddot{U}^{p-1}\} + \psi\,\Delta t^p\{\ddot{U}^p\} \tag{26}$$

where $\gamma$ and $\psi$ are numerical parameters determining the stability and accuracy characteristics of the Newmark method.[22]

Altogether, the equation to be solved for the current displacement vector $\{U^p\}$ is

$$\begin{aligned}\left[\frac{2}{\gamma(\Delta t^p)^2}[M] + \sum_{r=1}^{4}\left(Q_r^{\infty} + \sum_{\rho=1}^{N_r}\bar{S}_{r\rho}^p Q_{r\rho}\right)[K_r]\right]\{U^p\} &= \{F^p\} + [M]\left\{\frac{2}{\gamma(\Delta t^p)^2}\{U^{p-1}\} + \frac{2}{\gamma\Delta t^p}\{\dot{U}^{p-1}\}\right.\\ &\left. + \left(\frac{1}{\gamma} - 1\right)\{\ddot{U}^{p-1}\}\right\}\\ &- \sum_{r=1}^{4}\sum_{\rho=1}^{N_r}\left\{R_{r\rho}^p\right\} + \sum_{r=1}^{4}\left(\sum_{\rho=1}^{N_r}\bar{S}_{r\rho}^p Q_{r\rho}\right)[K_r]\{U^{p-1}\}\\ &+ \sum_{r=1}^{4}Q_r^{\infty}\left[\theta_T^p\left\{F_r^T\right\} + \theta_H^p\left\{F_r^H\right\}\right]\\ &+ \sum_{r=1}^{4}\left(\sum_{\rho=1}^{N_r}\bar{S}_{r\rho}^p Q_{r\rho}\right)\left[\Delta\theta_T^p\left\{F_r^T\right\} + \Delta\theta_H^p\left\{F_r^H\right\}\right]\end{aligned} \tag{27}$$

where

$$\begin{aligned}\left\{R_{r\rho}^p\right\} &= \int_{-\infty}^{t^{p-1}} Q_{r\rho}\exp\left(-\frac{\zeta_r^p - \zeta_r'}{\lambda_{r\rho}}\right)[K_r]\left\{\frac{\partial U}{\partial\tau}\right\}\mathrm{d}\tau\\ &- \int_{-\infty}^{t^{p-1}} Q_{r\rho}\exp\left(-\frac{\zeta_r^p - \zeta_r'}{\lambda_{r\rho}}\right)\frac{\partial\theta_T}{\partial\tau}\left\{F_r^T\right\}\mathrm{d}\tau\\ &- \int_{-\infty}^{t^{p-1}} Q_{r\rho}\exp\left(-\frac{\zeta_r^p - \zeta_r'}{\lambda_{r\rho}}\right)\frac{\partial\theta_H}{\partial\tau}\left\{F_r^H\right\}\mathrm{d}\tau\end{aligned} \tag{28}$$

Writing the expression for $\{R_{r\rho}^{p-1}\}$ and approximating the hereditary integrals from $t^{p-2}$ to $t^{p-1}$ in a similar manner to that shown in Eq. (22), the following recurrence relation is obtained for $\{R_{r\rho}^p\}$:

$$\left\{R_{r\rho}^p\right\} = \exp\left(-\Delta\zeta_r^p/\lambda_{r\rho}\right)\left[\left\{R_{r\rho}^{p-1}\right\} + \bar{S}_{r\rho}^{p-1}Q_{r\rho}\left([K_r]\{\Delta U^{p-1}\} - \Delta\theta_T^{p-1}\left\{F_r^T\right\} - \Delta\theta_H^{p-1}\left\{F_r^H\right\}\right)\right] \tag{29}$$

Hence, the displacement solution for the current time step is completely determined in terms of quantities from only the previous two time steps.

The following initial conditions are used:

$$\{U^0\} = \{0\}, \qquad \{\dot{U}^0\} = \{0\}, \qquad \{\ddot{U}^0\} = \{0\}, \qquad \bar{S}_{r\rho}^0 = 1$$
$$\theta_T^0 = 0, \qquad \theta_H^0 = 0, \qquad \left\{R_{r\rho}^0\right\} = \{0\} \tag{30}$$

For the case where the temperature and moisture are constant over a time step, the reduced time increment $\Delta\zeta_r^p$ is simply

$$\Delta\zeta_r^p = \frac{1}{A_r(T^p, H^p)}\Delta t^p \tag{31}$$

If the hygrothermal environment varies over a time step, $\Delta\zeta_r^p$ can be evaluated by numerically integrating $1/A_r$ over the time step, as indicated by Eq. (2).

The quasistatic equation for the current displacement is similar to Eq. (27), but with any of the terms multiplied by the mass matrix deleted. Either a lumped or what is termed a "consistent" mass matrix may be used in the calculations when inertia is to be included. If a lumped mass matrix is chosen, the mass associated with each translational DOF is simply one-third of the elemental mass. In that case, the rotary inertia associated with each node is neglected. If, however, a consistent mass matrix is chosen, the mass matrix including all terms corresponding to the rotary inertias is formulated as follows: The development of a consistent mass matrix for the transformed LST element presents no difficulties. However, because explicit shape functions for the transverse displacement $w$ are not used in the derivation of the DKT element, a further approximation in the derivation of a consistent bending mass matrix must be made. As described by Kapania and Mohan,[17] in addition to using the shape functions for $\theta_x$ and $\theta_y$, a nine-term polynomial in area coordinates is introduced to approximate the transverse displacement $w$ over an element, allowing a consistent bending mass matrix to be found.

Once the displacements for the time period of interest have been determined, the strains can be computed directly from Eq. (5). Using the constitutive law given by Eq. (4), the stress at a given point at a given time $t^p$ then is evaluated as

$$\begin{aligned}\{\sigma(t^p)\} &= \sum_{r=1}^{4}Q_r^{\infty}[D_r]\left\{\{e^p\} + z\{\kappa^p\} - \theta_T^p\{\alpha\} - \theta_H^p\{\beta\}\right\}\\ &+ \sum_{r=1}^{4}\sum_{\rho=1}^{N_r}\bar{S}_{r\rho}^p Q_{r\rho}[D_r]\left\{\{\Delta e^p\} + z\{\Delta\kappa^p\} - \Delta\theta_T^p\{\alpha\}\right.\\ &\left. - \Delta\theta_H^p\{\beta\}\right\} + \sum_{r=1}^{4}\sum_{\rho=1}^{N_r}\left\{W_{r\rho}^p\right\}\end{aligned} \tag{32}$$

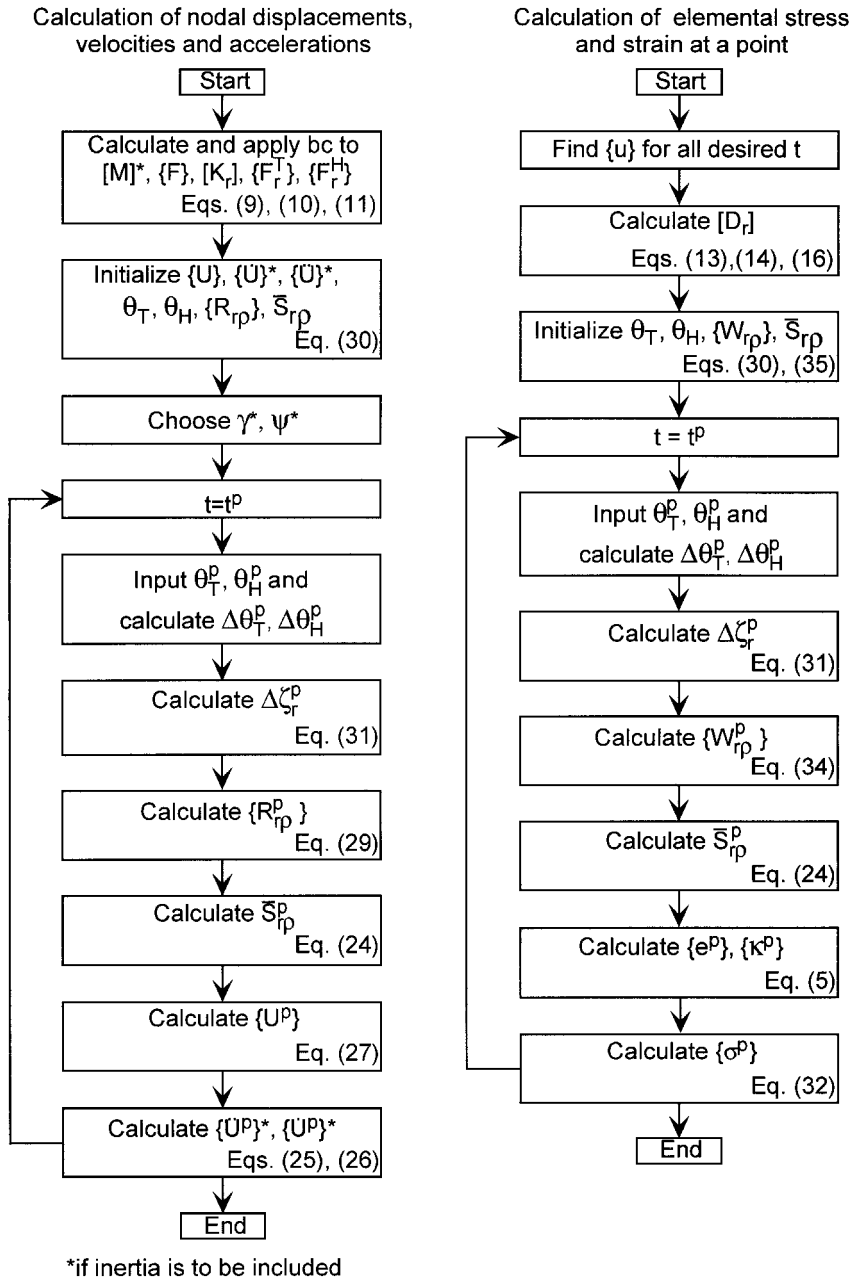


**Fig. 2 Solution procedures used in determining desired nodal and elemental quantities.**

where

$$\{W_{r\rho}^{p}\} = \int_{-\infty}^{t_{p-1}} \exp\left(-\frac{\zeta_r^p - \zeta_r'}{\lambda_{r\rho}}\right) Q_{r\rho}[D_r]\left\{\left\{\frac{\partial e}{\partial \tau}\right\} + z\left\{\frac{\partial \kappa}{\partial \tau}\right\} - \frac{\partial \theta_T}{\partial \tau}\{\alpha\} - \frac{\partial \theta_H}{\partial \tau}\{\beta\}\right\} d\tau \tag{33}$$

$$= \exp\left(-\frac{\Delta\zeta_r^p}{\lambda_{r\rho}}\right)\left[\{W_{r\rho}^{p-1}\} + \bar{S}_{r\rho}^{p-1} Q_{r\rho}[D_r]\{\{\Delta e^{p-1}\} + z\{\Delta\kappa^{p-1}\} - \Delta\theta_T^{p-1}\{\alpha\} - \Delta\theta_H^{p-1}\{\beta\}\}\right] \tag{34}$$

with the initial condition

$$\{W_{r\rho}^{0}\} = \{0\} \tag{35}$$

Shown in Fig. 2 are flowcharts for the procedures necessary to calculate the nodal displacements, velocities, and accelerations and the elemental stresses and strains. Note that the global nodal displacements $\{U\}$ for the total time considered are found first, with the elemental stresses and strains found afterward, if desired. The relevant equation numbers are indicated.

## Numerical Examples

From this point forward, the developed finite element is termed TVATDKT (thermoviscoelastic, Allman triangle, discrete Kirchhoff theory). Five example problems are presented to demonstrate the capability and verify the accuracy of the TVATDKT element in its current stage of development. First, the quasistatic and dynamic responses of an isotropic cantilever subjected to a tip load are determined. Numerical results for the quasistatic deflection and stress response of a simply supported viscoelastic $[0/90]_s$ composite plate under a uniform pressure load then are presented. The strain response of a free viscoelastic composite plate subjected to a uniform edge load applied instantaneously at $t = 0$ and removed instantaneously at $t = 24$ h follows. Several stacking sequences are considered. Next, the response of one of these plates subjected to a uniform temperature change is given. Finally, numerical results are presented for two composite viscoelastic cylindrical panels that are both subjected to a uniform pressure load.

### Viscoelastic Cantilever with Tip Load

A tip load $P_0 = 0.1$ N is suddenly applied at $t = 0$ and held constant thereafter. The beam has dimensions of $1.0 \times 0.3$ m and

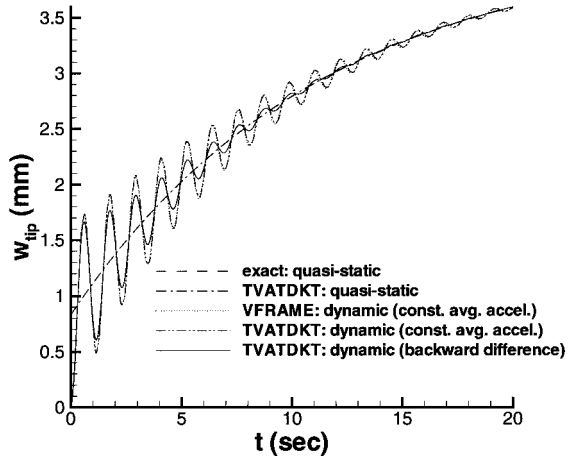


**Fig. 3 Quasistatic and dynamic tip deflection of cantilever beam under suddenly applied tip force.**

a thickness of 0.0254 m. The material is represented as a three-parameter solid with the relaxation modulus given by

$$E(t) = 1.96 \times 10^7 + 7.84 \times 10^7 e^{-t/2.24} \text{ N/m}^2 \tag{36}$$

where $t$ is in seconds. The material density is 2200 kg/m$^3$.

Shown in Fig. 3 are the quasistatic and dynamic results for the cantilever tip deflection. The exact quasistatic solution for the tip deflection is computed using the correspondence principle[23] as

$$w_{\text{tip}} = \left(P_0 L^3 / 3I\right) D_c(t) \tag{37}$$

where $L$ and $I$ are the beam's length and cross-sectional moment of inertia, respectively, and $D_c(t)$ is the creep compliance. Setting $\nu = 0$ and computing the $Q_r(t)$ using the expression given by Eq. (36) for $E(t)$ allows the flat shell element code to be used to model the cantilever beam. Quasistatic and dynamic results for the tip deflection are computed using 30 TVATDKT elements. For the dynamic case, a lumped mass matrix is employed in the TVATDKT code. The dynamic results also are computed using a completely independent, linear viscoelastic plane-frame element code, VFRAME, developed by the present authors. For the VFRAME code, the viscoelastic equations are marched in time utilizing the Newmark method for the inertia term in conjunction with a direct integration scheme for the viscoelastic memory loads similar to that proposed by White.[5] A total of 10 VFRAME elements are used. For the dynamic case, the constant average acceleration method ($\gamma = \psi = 1/2$) with $\Delta t = 0.01$ s is used with the VFRAME and TVATDKT formulations. Implementing the constant average acceleration method with $\Delta t = 0.001$ s did not appreciably change either the VFRAME or the TVATDKT results. In Fig. 3, the differences between the TVATDKT and exact results for the quasistatic case and between the TVATDKT and VFRAME dynamic results using the constant average acceleration method cannot be distinguished. The maximum acceleration corresponding to $w_{\text{tip}}$ computed for the dynamic case using the TVATDKT formulation and the constant average acceleration method is 101.25 mm/s$^2$.

The dynamic results oscillate about the quasistatic results with an amplitude of vibration that decreases as time evolves, because of the viscoelastic damping. In general, the amplitude of the oscillations depends upon the material density, the rate at which the loading is applied and the amount of viscoelastic damping.

A poor choice of $\gamma$ and $\psi$ for the Newmark method can lead to undesired numerical damping for a given time-step size, as exhibited by the dynamic results shown in Fig. 3 produced using the TVATDKT formulation with the backward difference method ($\gamma = 2$, $\psi = \frac{3}{2}$) and $\Delta t = 0.01$ s.

**Square Viscoelastic [0/90]$_s$ Composite Plate Under Pressure Load**

The length of each side is 10 m, while the plate thickness is 0.1 m. The boundary conditions are taken as simply supported. A uniform pressure load of $q_0 = 1$ N/m$^2$ is suddenly applied at $t = 0$ and held constant thereafter. The material relaxation moduli are assumed as follows:

$$\begin{gathered} E_1 = 9.8 \times 10^7 \text{ N/m}^2 \\ E_2(t) = (1.96 + 7.84\, e^{-t/2.24} + e^{-t/10}) \times 10^5 \text{ N/m}^2 \\ \nu_{12} = 0.25 \\ G_{12}(t) = (0.98 + 3.92\, e^{-t/2.24} + 0.5\, e^{-t/10}) \times 10^5 \text{ N/m}^2 \end{gathered} \tag{38}$$

where $t$ is in seconds. This will give the fiber-dominated relaxation modulus $Q_1$ as elastic (constant in time) and the other three relaxation moduli, $Q_2$–$Q_4$, which are matrix-dominated, as viscoelastic.

The exact quasistatic response for the transverse deflection can be determined once again using the correspondence principle and is given by

$$w(x, y, t) = \mathcal{L}^{-1}\left\{ \frac{16 q_0}{\pi^6 s^2} \sum_{m=1,3,5}^{\infty} \sum_{n=1,3,5}^{\infty} \frac{(1/mn)\sin(m\pi x/L)\sin(n\pi y/L)}{\hat{D}_{11}(m/L)^4 + 2(\hat{D}_{12} + 2\hat{D}_{66})(m/L)^2(n/L)^2 + \hat{D}_{22}(n/L)^4} \right\} \tag{39}$$

where $\mathcal{L}$ is the Laplace operator, $\hat{(\cdot)}$ denotes the Laplace transform of $(\cdot)$, and $s$ is the Laplace variable. A total of 36 terms in the Fourier series was sufficient to give accurate results for the initial and final ($t = \infty$) viscoelastic midpoint deflection; using 100 terms only changed both results by slightly more than 0.0012%. Hence, using 36 terms to compute the "exact" solution for all times considered is acceptable and is performed. In this example and all other examples where needed, partial fraction expansions in the Laplace domain and inverse Laplace transforms are computed exactly utilizing the commercial software package MATHEMATICA.[24]

Using the resulting expression for $w(x, y, t)$, the bending curvature vector $\{\kappa\}$ is found and the stresses are computed as follows:

$$\{\sigma(t)\} = \int_0^t z[\bar{Q}(t-\tau)]\left\{\frac{\partial \kappa}{\partial \tau}\right\} d\tau = \mathcal{L}^{-1}\{sz[\hat{\bar{Q}}(s)]\{\hat{\kappa}(s)\}\} \tag{40}$$

The TVATDKT results for the midpoint transverse deflection $w_{\text{mid}}$ and $\sigma_x$ at $z = z_{\max}$ using 72, 200, and 512 elements with $\Delta t = 0.1$ s are shown in Fig. 4, along with exact values computed by applying the correspondence principle. For the 200-element mesh, using $\Delta t = 0.01$ s did not significantly change the results. The TVATDKT results appear to converge to the exact solution.

**Free Viscoelastic Laminated Plate Under Edge Load**

The plate dimensions are 1.0 × 2.0 in. Each layer has a thickness of 0.02 in. with the following material properties (matching a Gr/Ep) at the instant the plate is loaded:

$$\begin{gathered} E_1 = 18 \text{ Msi}, \qquad G_{12} = 0.9 \text{ Msi}, \qquad \alpha_1 = 0.2 \times 10^{-6}/^\circ\text{F} \\ E_2 = 1.4 \text{ Msi}, \qquad \nu_{12} = 0.34, \qquad \alpha_2 = 16.0 \times 10^{-6}/^\circ\text{F} \end{gathered} \tag{41}$$

Once again, $E_1$ is taken as fiber-dominated and constant in time. Hence, $Q_1$ also will be constant in time. The other $Q_r$ then are computed as

$$Q_r(t) = Q_r(0)\, f(t) \quad \text{where} \quad f(t) = f_0 + \sum_{i=1}^{10} f_i e^{-t/\lambda_i} \tag{42}$$

The values given in Table 1 for $f_i$ and $\lambda_i$ are those listed by Lin and Hwang,[10] which are a data fit to relaxation data presented by Crossman et al.[2] A uniform edge load of $N_x = 276.48$ lb/in. is applied at $t = 0$ and held constant until $t = 24$ h, at which point it is suddenly removed.

Because of symmetry, only one-fourth of the plate is analyzed using two elements. The quasistatic strain results for several stacking sequences ($[\pm 45/0/90]_s$, $[\pm 45_2]_s$, and $[(0/90)_2]_s$) are shown in Fig. 5a for $\Delta t = 100$ s. As expected for this loading, the $[\pm 45_2]_s$

**Table 1 Components of normalized function giving viscoelastic Gr/Ep property time variation**

| $i$ | $f_i$ | $\lambda_i$, s |
|---|---|---|
| 0 | 0.06698253 | |
| 1 | 0.0729459 | $8.174141919 \times 10^{15}$ |
| 2 | 0.0696426 | $4.976486103 \times 10^{14}$ |
| 3 | 0.150514 | $1.477467149 \times 10^{13}$ |
| 4 | 0.148508 | $4.761315266 \times 10^{11}$ |
| 5 | 0.146757 | $1.799163029 \times 10^{10}$ |
| 6 | 0.102892 | $5.253922053 \times 10^{8}$ |
| 7 | 0.114155 | $1.846670914 \times 10^{7}$ |
| 8 | 0.071036 | $5.288067476 \times 10^{5}$ |
| 9 | 0.0484272 | $1.494783951 \times 10^{4}$ |
| 10 | 0.00813977 | $5.516602214 \times 10^{2}$ |

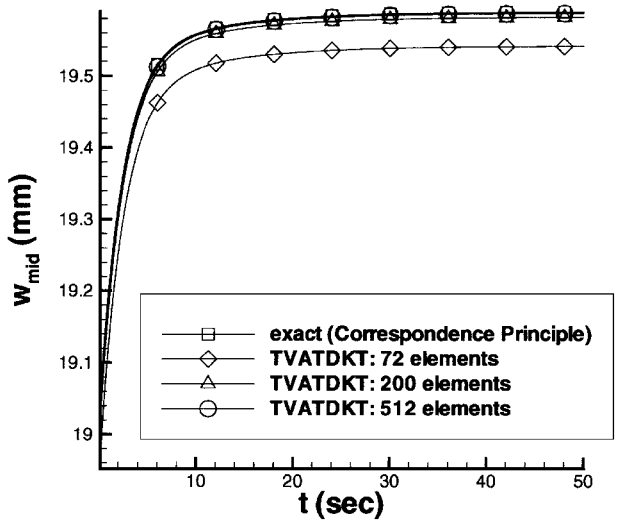


**a) Midpoint transverse deflection, $w_{mid}$**

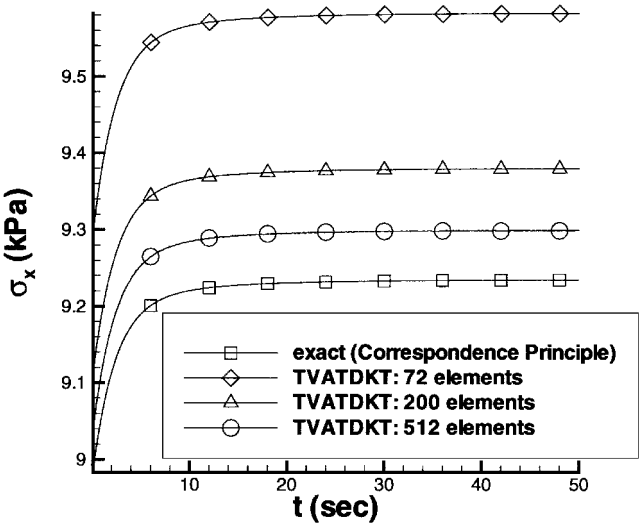


**b) Midpoint $\sigma_x$ at $z = z_{max}$**

**Fig. 4 Simply supported square viscoelastic $[0/90]_s$ composite plate under uniform pressure load.**

plate shows the most time dependence in its response because the matrix for this stacking sequence carries a larger percentage of the load than those for the other stacking sequences.

The exact quasistatic strain solution for the $[\pm 45_2]_s$ laminate is computed as follows: For this laminate, the only nonzero stress in each layer is simply

$$\sigma_x(t) = 1728[u(t) - u(t - 24\,\text{h})]\ \text{psi} \tag{43}$$

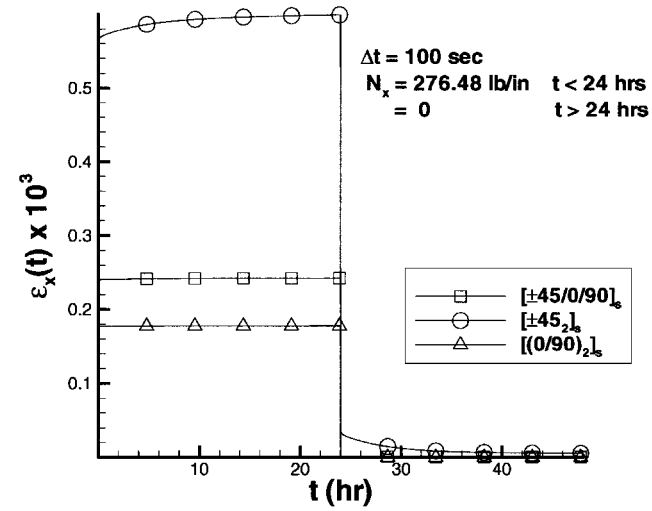


**a) $[\pm 45/0/90]_s$, $[\pm 45_2]_s$, and $[(0/90)_2]_s$ with $\Delta t = 100$ s**

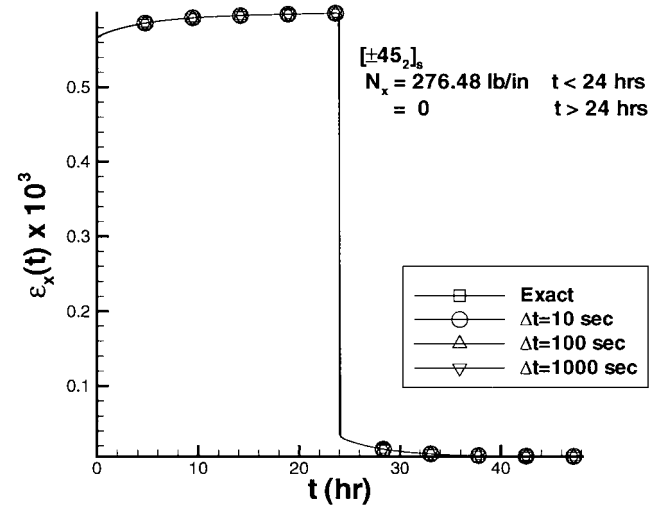


**b) $[\pm 45_2]_s$ with $\Delta t = 10$, 100, and 1000 s**

**Fig. 5 Free viscoelastic composite plates subjected to sudden loading and unloading.**

where $u(t)$ is the unit step function. The Laplace transform of the constitutive law then is used to calculate $\hat{\epsilon}_x(s)$. This result can be simplified to give

$$\epsilon_x(t) = \mathcal{L}^{-1}\left\{\frac{\hat{\sigma}_x}{s}\left[\frac{1}{4\hat{Q}_4} + \frac{1}{\hat{Q}_1 + 2\hat{Q}_2 + \hat{Q}_3}\right]\right\} \tag{44}$$

As shown in Fig. 5b, the computed TVATDKT results using $\Delta t = 10$, 100, and 1000 s are all in excellent agreement with the exact solution.

**Free Viscoelastic Laminated Plate Under Thermal Load**

Now consider the $[\pm 45/0/90]_s$ plate of the preceding example to be subjected to a uniform change in temperature applied at $t = 0$ and held constant thereafter. The temperature for zero thermal strain is taken as 350°F. Temperature changes of −275°F and −190°F are considered. The shift factors for $Q_2$, $Q_3$, and $Q_4$ are taken to be the same and are given as 1.0 and 1.51357E-5 for $T = 75$°F and $T = 160$°F, respectively, which are taken from Lin and Hwang.[10] Once again, two elements are used to model one-fourth of the plate because using a higher number of elements does not alter the solution greatly. Shown in Figs. 6a and 6b are the results for the stress in the 0-deg layer and the strain normalized by their initial values, along with some of the results given by Lin and Hwang.[11] In the present analysis, a time-step size of $\Delta t = 400$ s is used. From the TVATDKT calculations, the initial $\sigma_x$ and $\epsilon_x$ values, respectively, are −5380.0 psi and $-4.55512 \times 10^{-4}$ for $\Delta T = -275$°F, whereas for $\Delta T = -190$°F, the initial stress and strain values are −3717.1 psi

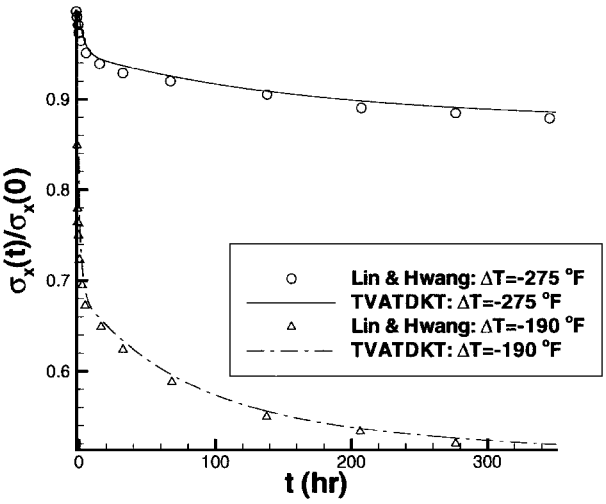


**a) Normalized $\sigma_x$ in 0-deg layer**

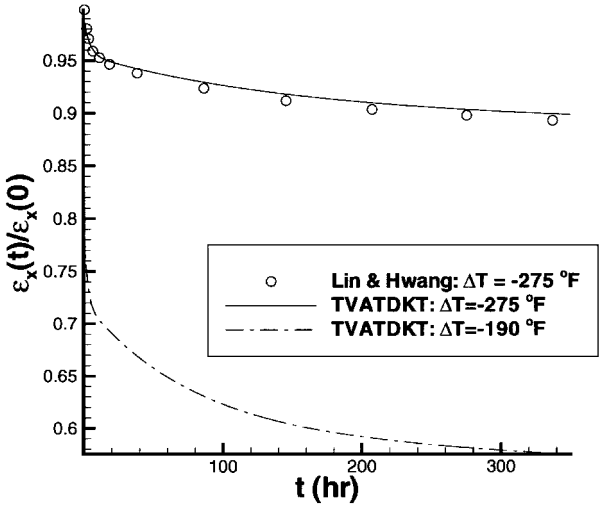


**b) Normalized $\epsilon_x$**

**Fig. 6 Free viscoelastic $[\pm 45/0/90]_s$ plate subjected to uniform $\Delta T$ applied at $t = 0$ and held constant thereafter.**

and $-3.14717 \times 10^{-4}$, respectively. Lin and Hwang[11] computed initial stress values of $-5380$ psi and $-3717$ psi for $\Delta T = -275$°F and $\Delta T = -190$°F, respectively, with an initial strain value of $-4.56 \times 10^{-4}$ for $\Delta T = -275$°F. Good agreement exists between the present and previously published results. Finally, it is observed that the thermorheologically simple viscoelastic response of the plate is a nonlinear function of the plate's temperature.

### Viscoelastic Composite Cylindrical Panels Under Pressure Load

Two cylindrical panels differing only in the panel half-angle are subjected to a uniform pressure load $q_0 = 0.3$ psi, which is applied suddenly at $t = 0$ and held constant thereafter. The length of both panels is 80 in. and the arc length of the other side is either 41.89 or 62.83 in., corresponding respectively to half-angles of $\phi = 12$ and 18 deg and a radius of 100 in. On each edge, both cylindrical panels rest on diaphragms that are rigid in their plane but perfectly flexible otherwise. The cross-ply stacking sequence is $[0/90]_s$ with the thickness of each layer taken to be 0.08 in., giving a total laminate thickness of 0.32 in. The properties at the initial time match those given in Eq. (41) for a Gr/Ep. Once again, $Q_1$ is assumed to be fiber dominated and constant in time. However, the $Q_2$–$Q_4$ relaxation functions are determined from[25]

$$E_2(t) = (116.333 + 6.02203\,e^{-t/287.154} + 10.8854\,e^{-t/5512.77} + 6.75662\,e^{-t/113,384}) \times 10^4 \text{ psi} \quad (45)$$

$$G_{12}(t) = (75.9301 + 3.86299\,e^{-t/287.154} + 6.3555\,e^{-t/5512.77} + 3.85226\,e^{-t/113,384}) \times 10^4 \text{ psi} \quad (46)$$

where $t$ is in minutes.

A closed-form solution for this problem using shallow shell theory is computed as follows. Let $v_1$, $v_2$, and $v_3$ be the translational displacements in the direction of the three shell coordinates. The first shell coordinate $\xi_1$ varies along the direction having zero curvature, whereas the second shell coordinate $\xi_2$ varies along the direction having constant nonzero curvature. The third shell coordinate $\xi_3$ (the shell normal) is determined from the right-hand rule and points away from the center of curvature of the $\xi_1$-constant arcs. As chosen, the shell coordinates are principal coordinates. Using the Love–Kirchhoff hypothesis and other approximations appropriate for thin elastic laminated shallow shells as described by Leissa and Qatu,[26] the governing equations in terms of $v_1$, $v_2$, and $v_3$ for a shallow elastic cylindrical panel with a symmetric cross-ply stacking sequence under uniform pressure are

$$A_{11}v_{1,11} + A_{12}[v_{2,12} + (v_{3,1}/R_2)] + A_{66}(v_{1,22} + v_{2,12}) = 0 \quad (47)$$

$$A_{12}v_{1,12} + A_{22}[v_{2,22} + (v_{3,2}/R_2)] + A_{66}(v_{1,12} + v_{2,11}) = 0 \quad (48)$$

$$A_{12}(v_{1,1}/R_2) + A_{22}\left[(v_{2,2}/R_2) + \left(v_3/R_2^2\right)\right] + D_{11}v_{3,1111} + 2(D_{12} + 2D_{66})v_{3,1122} + D_{22}v_{3,2222} = q_3 \quad (49)$$

Here $R_2$ is the radius associated with the panel and $(\cdot)_{,i}$ denotes differentiation with respect to shell coordinate $\xi_i$.

The uniform pressure load $q_3$ is written as

$$q_3 = q_0 = \sum_{m=1,3,5}^{\infty} \sum_{n=1,3,5}^{\infty} \frac{16q_0}{\pi^2 mn} \sin\frac{m\pi\xi_1}{l_1} \sin\frac{n\pi\xi_2}{l_2} \quad (50)$$

The boundary conditions are

$$\xi_1 = 0, l_1: \quad v_2 = v_3 = 0 \quad \text{and} \quad N_{11} = 0, \quad M_{11} = 0 \quad (51)$$

$$\xi_2 = 0, l_2: \quad v_1 = v_3 = 0 \quad \text{and} \quad N_{22} = 0, \quad M_{22} = 0 \quad (52)$$

where $N_{ij}$ and $M_{ij}$ are the usual force and force-couple resultants. Using the constitutive law, the strain-displacement relations and the conditions on $v_1$–$v_3$ given above, the boundary conditions can be written strictly in terms of $v_1$–$v_3$ as

$$\xi_1 = 0, l_1: \quad v_2 = v_3 = 0 \quad \text{and} \quad v_{1,1} = 0, \quad v_{3,11} = 0 \quad (53)$$

$$\xi_2 = 0, l_2: \quad v_1 = v_3 = 0 \quad \text{and} \quad v_{2,2} = 0, \quad v_{3,22} = 0 \quad (54)$$

The boundary conditions and governing equations are satisfied exactly by the following Fourier series expansions:

$$v_1 = \sum_{m=1,3,5}^{\infty} \sum_{n=1,3,5}^{\infty} I_{mn} \cos\frac{m\pi\xi_1}{l_1} \sin\frac{n\pi\xi_2}{l_2} \quad (55)$$

$$v_2 = \sum_{m=1,3,5}^{\infty} \sum_{n=1,3,5}^{\infty} J_{mn} \sin\frac{m\pi\xi_1}{l_1} \cos\frac{n\pi\xi_2}{l_2} \quad (56)$$

$$v_3 = \sum_{m=1,3,5}^{\infty} \sum_{n=1,3,5}^{\infty} K_{mn} \sin\frac{m\pi\xi_1}{l_1} \sin\frac{n\pi\xi_2}{l_2} \quad (57)$$

The constant coefficients $I_{mn}$, $J_{mn}$, and $K_{mn}$ for the elastic case are determined by substituting Eqs. (55), (56), and (57) into Eqs. (47), (48), and (49) and solving. The viscoelastic results then are computed using the correspondence principle by replacing $A_{ij}$ and $D_{ij}$ with $s\hat{A}_{ij}(s)$ and $s\hat{D}_{ij}(s)$, respectively, and $q_0$ with $q_0/s$, and then taking the inverse Laplace transform. A total of 49 Fourier terms is used to compute the shallow shell theory results, with the results for

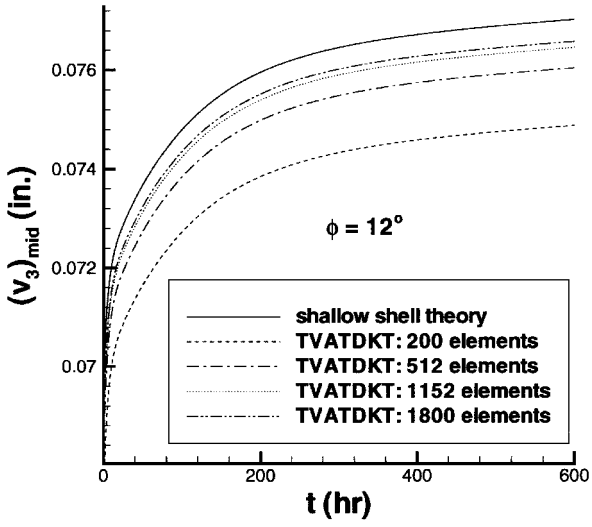


a) Panel with 12-deg half-angle

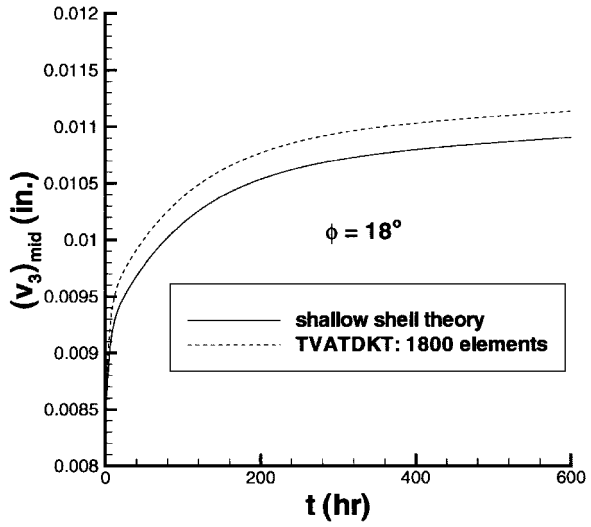


b) Panel with 18-deg half-angle

**Fig. 7 Midpoint transverse deflection $(v_3)_{mid}$ for viscoelastic $[0/90]_s$ cylindrical panels subjected to a step uniform pressure load.**

$(v_3)_{mid}$ at $t = 0$ for the $\phi = 12$-deg and $\phi = 18$-deg panels, respectively, being slightly less than 0.007% and 0.12% different than the results computed using 100 Fourier terms.

For both panels, a time-step size of $\Delta t = 100$ min is used. The time history of the midpoint deflection for the $\phi = 12$-deg panel is shown in Fig. 7a for several mesh sizes. The convergence appears to be reasonable, with the error remaining for the 1800-element case approximately equal to $-0.6\%$ for large $t$. Shown in Fig. 8 are plots of the closed-form and 1800-element TVATDKT results for the $v_3$ deflection at $\xi_1 = x = 0.5\, l_1$ for $t = 100$ min and $t = 600$ h. The deformation pattern is such that a single extremum exists at the panel center.

The cylindrical panel with the 18-deg half-angle is discretized using 1800 elements. The original undeformed mesh is shown in Fig. 9a, whereas the deformed mesh at $t = 600$ h is shown in Fig. 9b. To ascertain the deformation pattern, the displacements were scaled by a factor of 300 in Fig. 9b. Note that, when $\xi_2 = 0.5\, l_2$, the shell coordinate system is aligned with the $x$-$y$-$z$ global coordinate system shown in Figs. 9a and 9b.

Shown in Figs. 10a and 10b are plots of the shallow shell theory and TVATDKT values for the $v_3$ deflection for the section at $\xi_1 = x = 0.5\, l_1$ for $t = 100$ min and $t = 600$ h, respectively. As time evolves, the $v_3$ deformations tend to increase as the shell undergoes creep deformations, which can be observed by comparing Figs. 10a and 10b. Figure 7b shows the TVATDKT and shallow shell theory results for the time history of the transverse deflection at the shell

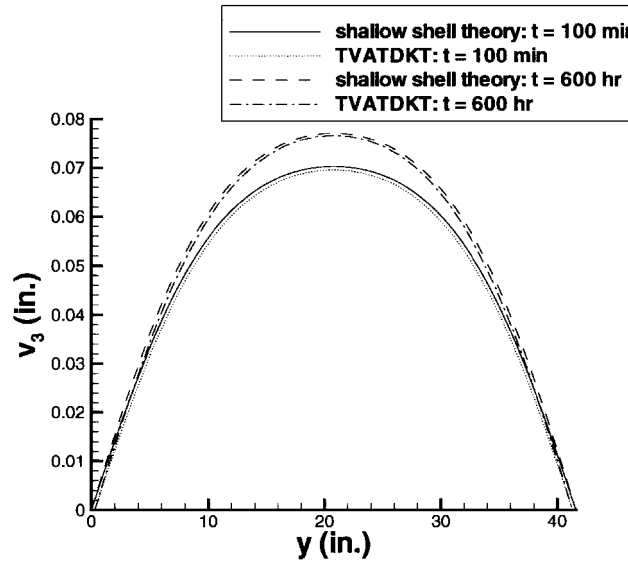


**Fig. 8 Transverse deflection $v_3$ at panel midsection $(\xi_1 = 1/2 l_1)$ of a viscoelastic $[0/90]_s$ cylindrical panel with 12-deg half-angle subjected to a step uniform pressure load. Results are shown for $t = 100$ min and $t = 600$ h.**

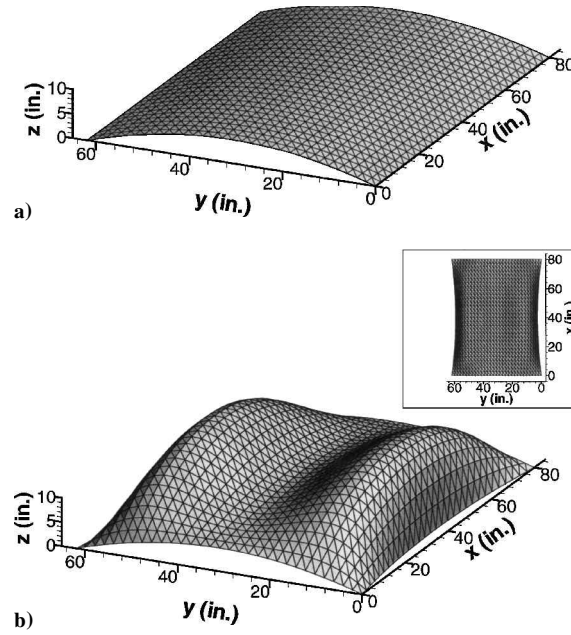


**Fig. 9 Viscoelastic $[0/90]_s$ cylindrical panel with 18-deg half-angle subjected to step uniform pressure: a) undeformed mesh, b) deformed mesh at $t = 600$ h with displacements multiplied by 300.**

midpoint $(v_3)_{mid}$. The deformed shape of the shell at any given time is similar to that shown in Fig. 9b. The applied pressure causes the two $\xi_2$-constant edges to be pulled toward the panel center, whereas the two $\xi_1$-constant edges are pushed away from the panel center, but to a lesser extent. Because of the applied boundary conditions, the four corners do not translate. The two peaks in the deformation move slightly inward as time evolves, whereas the center trough remains stationary because of symmetry. The differences between the shallow shell theory and finite element results for this panel are somewhat larger than those for the $\phi = 12$-deg panel for several likely reasons. First, using 1800 elements for the $\phi = 18$-deg panel gives a slightly larger element size than using 1800 elements for the $\phi = 12$-deg panel. Second, the adequacy of shallow shell theory for this problem decreases as the shell becomes deeper, i.e., as the panel half-angle increases. Finally, the deformation pattern is more complex for the $\phi = 18$-deg panel than for the $\phi = 12$-deg panel.

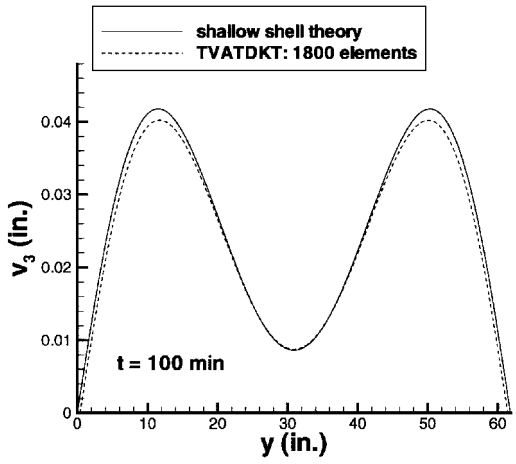


a) $t = 100$ min

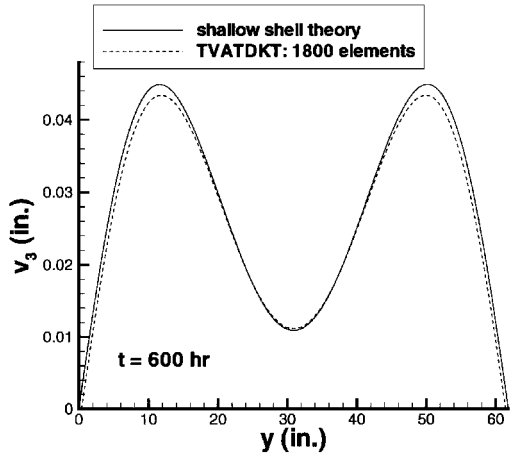


b) $t = 600$ h

**Fig. 10 Transverse deflection $v_3$ at panel midsection ($\xi_1 = 1/2l_1$) of a viscoelastic $[0/90]_s$ cylindrical panel with 18-deg half-angle subjected to a step uniform pressure load.**

## Summary and Conclusions

The geometrically linear dynamic analysis capability of an elastic flat shell element has been extended to include thermoviscoelasticity. The element is the combination of the DKT plate bending element and a membrane element similar to the AT element, but derived by transferring the midside translations of the LST element to corner node translations and rotations. Prony series are used to represent the relaxation moduli for linearly viscoelastic behavior, whereas reduced timescales are used to model hygrothermorheologically simple materials. The hygrothermal loads also are included in the formulation. Recursion relationships are employed to evaluate the resulting hereditary integrals, and the Newmark time integration scheme is implemented to incorporate inertial effects.

The results produced using the present formulation agreed well with solutions determined using the correspondence principle and results available in the existing literature for mechanical loads, thermal loads, and load removal. For the case of a cantilever under a tip load, the dynamic results from the present formulation matched the results obtained from an independent viscoelastic plane-frame element code developed by the present authors.

## Acknowledgments

Daniel Hammerand was supported during this research by a National Science Foundation Graduate Research Fellowship. The support for Rakesh Kapania during this research was provided by Grant DAAH04-95-1-0175 from the Army Research Office with Gary Anderson as the grant monitor and is greatly appreciated. We would like to thank Bernard Grossman, Department Head, Aerospace and Ocean Engineering, for providing considerable computational resources. We would also like to thank Raymond Plaut, Department of Civil and Environmental Engineering, and P. Mohan and Jing Li, Department of Aerospace and Ocean Engineering, for valuable discussions held during the course of this research.

## References

[1] Aklonis, J. J., and MacKnight, W. J., *Introduction to Polymer Viscoelasticity*, 2nd ed., Wiley, New York, 1983.

[2] Crossman, F. W., Mauri, R. E., and Warren, W. J., "Moisture-Altered Viscoelastic Response of Graphite/Epoxy Composites," *Advanced Composite Materials—Environmental Effects*, STP 658, American Society for Testing and Materials, Philadelphia, PA, 1978, pp. 205–220.

[3] Lee, E. H., and Rogers, T. G., "Solution of Viscoelastic Stress Analysis Problems Using Measured Creep or Relaxation Functions," *Journal of Applied Mechanics*, Vol. 30, No. 1, 1963, pp. 127–133.

[4] Zak, A. R., "Structural Analysis of Realistic Solid-Propellant Materials," *Journal of Spacecraft and Rockets*, Vol. 5, No. 3, 1967, pp. 270–275.

[5] White, J. L., "Finite Elements in Linear Viscoelasticity," *Proceedings of 2nd Conference on Matrix Methods in Structural Mechanics*, U.S. Air Force Flight Dynamics Lab., AFFDL-TR-68-150, Wright–Patterson AFB, Dayton, OH, 1968, pp. 489–516.

[6] Taylor, R. L., Pister, K. S., and Goudreau, G. L., "Thermomechanical Analysis of Viscoelastic Solids," *International Journal for Numerical Methods in Engineering*, Vol. 2, No. 1, 1970, pp. 45–59.

[7] Wang, Y. Z., and Tsai, T. J., "Static and Dynamic Analysis of a Viscoelastic Plate by the Finite Element Method," *Applied Acoustics*, Vol. 25, No. 2, 1988, pp. 77–94.

[8] Ben-Zvi, R., "A Simple Implementation of a 3D Thermo-Viscoelastic Model in a Finite Element Program," *Computers and Structures*, Vol. 34, No. 6, 1990, pp. 881–883.

[9] Krishna, A., Harper, B. D., and Lee, J. K., "Finite Element Viscoelastic Analysis of Temperature and Moisture Effects in Electronic Packaging," *Journal of Electronic Packaging*, Vol. 117, No. 3, 1995, pp. 192–200.

[10] Lin, K. Y., and Hwang, I. H., "Thermo-Viscoelastic Response of Graphite/Epoxy Composites," *Journal of Engineering Materials and Technology*, Vol. 110, No. 2, 1988, pp. 113–116.

[11] Lin, K. Y., and Hwang, I. H., "Thermo-Viscoelastic Analysis of Composite Materials," *Journal of Composite Materials*, Vol. 23, June 1989, pp. 554–569.

[12] Hilton, H., and Yi, S., "Dynamic Finite Element Analysis of Viscoelastically Damped Composite Structures," *Applications of Supercomputers in Engineering II*, edited by C. A. Brebbia, D. Howard, and A. Peters, Computational Mechanics Publications, Elsevier Applied Science, London, 1991, pp. 495–511.

[13] Yi, S., and Hilton, H., "Dynamic Finite Element Analysis of Viscoelastic Composite Plates in the Time Domain," *International Journal for Numerical Methods in Engineering*, Vol. 37, No. 23, 1994, pp. 4081–4096.

[14] Yi, S., Ahmad, M. F., and Ramesh, A., "Data Parallel Computation for Thermo-Viscoelastic Analysis of Composite Structures," *Advances in Engineering Software*, Vol. 27, No. 1–2, 1996, pp. 97–102.

[15] Lin, K. Y., and Yi, S., "Analysis of Interlaminar Stresses in Viscoelastic Composites," *International Journal of Solids and Structures*, Vol. 27, No. 7, 1991, pp. 929–945.

[16] Yi, S., and Hilton, H., "Hygrothermal Effects on Viscoelastic Responses of Laminated Composites," *Composites Engineering*, Vol. 5, No. 2, 1995, pp. 183–193.

[17] Kapania, R. K., and Mohan, P., "Static, Free Vibration and Thermal Analysis of Composite Plates and Shells Using a Flat Triangular Shell Element," *Computational Mechanics*, Vol. 17, No. 5, 1996, pp. 343–357.

[18] Batoz, J. L., Bathe, K. J., and Ho, L. W., "A Study of Three-Node Triangular Plate Bending Elements," *International Journal for Numerical Methods in Engineering*, Vol. 15, No. 12, 1980, pp. 1771–1812.

[19] Allman, D. J., "A Compatible Triangular Element Including Vertex Rotations for Plane Elasticity Analysis," *Computers and Structures*, Vol. 19, No. 1–2, 1984, pp. 1–8.

[20] Ertas, A., Krafcik, J. T., and Ekwaro-Osire, S., "Performance of an Anisotropic Allman/DKT 3-Node Thin Triangular Flat Shell Element," *Composites Engineering*, Vol. 2, No. 4, 1992, pp. 269–280.

[21] Cook, R. D., "On the Allman Triangle and a Related Quadrilateral Element," *Computers and Structures*, Vol. 22, No. 6, 1986, pp. 1065–1067.

[22] Reddy, J. N., *An Introduction to the Finite Element Method*, 2nd ed., McGraw–Hill, New York, 1993.

[23] Christensen, R. M., *Theory of Viscoelasticity, An Introduction*, 2nd ed., Academic, New York, 1982.

[24] Wolfram, S., *The Mathematica Book*, 3rd ed., Cambridge Univ. Press, New York, 1996.

[25] Marques, S. P. C., and Creus, G. J., "Geometrically Nonlinear Finite Element Analysis of Viscoelastic Composite Materials Under Mechanical and Hygrothermal Loads," *Computers and Structures*, Vol. 53, No. 2, 1994, pp. 449–456.

[26] Leissa, A. W., and Qatu, M. S., "Equations of Elastic Deformation of Laminated Composite Shallow Shells," *Journal of Applied Mechanics*, Vol. 58, No. 1, 1991, pp. 181–188.

A. M. Waas
*Associate Editor*